Unraveling Hidden Charge Density Wave Phases in 1*T*-$TiSe_2$

Zhengwei Nie,[1,2] Yaxian Wang,[1,*] Daqiang Chen,[1,2] and Sheng Meng[1,2,3,†]
[1]*Beijing National Laboratory for Condensed Matter Physics and Institute of Physics, Chinese Academy of Sciences, Beijing 100190, China*
[2]*School of Physical Sciences, University of Chinese Academy of Sciences, Beijing 100190, China*
[3]*Songshan Lake Materials Laboratory, Dongguan, Guangdong 523808, China*

(Received 29 June 2023; accepted 2 October 2023; published 7 November 2023)

The unexpected chiral order observed in 1*T*-$TiSe_2$ represents an exciting area to explore chirality in condensed matter, while its microscopic mechanism remains elusive. Here, we have identified three metastable collective modes—the so-called single-*q* modes—in single layer $TiSe_2$, which originate from the unstable phonon eigenvectors at the zone boundary and break the threefold rotational symmetry. We show that polarized laser pulse is a unique and efficient tool to reconstruct the transient potential energy surface, so as to drive phase transitions between these states. By designing sequent layers with chiral stacking order, we propose a practical means to realize chiral charge density waves in 1*T*-$TiSe_2$. Further, the constructed chiral structure is predicted to exhibit circular dichroism as observed in recent experiments. These facts strongly indicate the chirality transfer from photons to the electron subsystem, meanwhile being strongly coupled to the lattice degree of freedom. Our work provides new insights into understanding and modulating chirality in quantum materials that we hope will spark further experimental investigation.

DOI: 10.1103/PhysRevLett.131.196401

In charge-ordered materials, the periodic modulation in electronic charge density is usually accompanied by a rearrangement of the underlying ionic lattice, forming so-called charge-density waves (CDWs) [1,2]. It reduces the translational symmetry of the system, and the coupling between electrons and atomic distortions may further trigger symmetry breaking in other degrees of freedom, resulting in emerging phases and orders. For example, CDW is correlated with the magnetic order in FeGe [3] and $Er_2Ir_3Si_5$ [4], and may account for the 3D quantum Hall effect in $ZrTe_5$ [5]. Besides, intriguing work has revealed intertwined CDW and superconductivity order in many unconventional superconductors [6–8].

In condensed matter physics, crystals are considered to be chiral when mirror reflection, space inversion, and rotoinversion symmetries are all broken [9,10]. In some cases, however, achiral lattices can host symmetry-breaking gyrotropic electronic order and form macroscopic chirality [11–14]. Therein, charge-density waves formed by the electron density modulation exhibit ubiquitous symmetry breaking, providing a unique platform to study chirality. Up to now, chiral CDWs have been observed in novel quantum materials such as $TiSe_2$ [15–20], TaS_2 [21–23], $NbSe_2$ [24], and KV_3Sb_5 [25]. In $TiSe_2$, the original reports of static chiral CDWs were detected as enantiomers with broken threefold rotational symmetry [18]. Later, an x-ray diffraction study indicates an emergent chiral atomic configuration occurring below the CDW transition temperature [15]. Recently, chiral CDWs with gyrotropic order are observed and manipulated via circularly polarized light, evidenced by the circular photogalvanic effect [20]. Despite these efforts, the microscopic origin of chiral CDW is still highly debated. Theoretically, a commonly held view is that there is a rotation of the dominant CDW propagation vectors as one travels from one layer to the next [14,26]. Besides, it is also suggested that a finite chirality may be resulted from a noncentrosymmetric CDW structure [19]. Therefore, a microscopic study of the chiral CDW in $TiSe_2$ is highly desired for deeper understanding and better manipulation of chirality at large.

Herein, we present a full *ab initio* study on the static and dynamical coupled electron-lattice order in $TiSe_2$ based on real-time time-dependent density-functional theory. We demonstrate that the CDW distorted pattern originates from the superposition of three rotationally invariant soft phonon modes and forms a triple-*q* mode, while laser excitations break such symmetry and selectively drive the formation of single-*q* modes. We show correspondence between such symmetry breakings and anisotropic Ti—Se bond weakening upon photoexcitation, as well as the resulting modulated potential energy surface. Further, an ultrafast laser pulse can induce and stabilize a selected metastable quantum phase. We then discuss the possibility to manipulate chiral CDW in $TiSe_2$ and construct bulk chiral structure by circularly polarized light. By simulating the circular dichroism of the illustrative model system we obtain similar results with previous observations. Our work provides new insights into the microscopic nature of chiral CDW in $TiSe_2$ and may further facilitate engineering charge ordering in quantum materials.

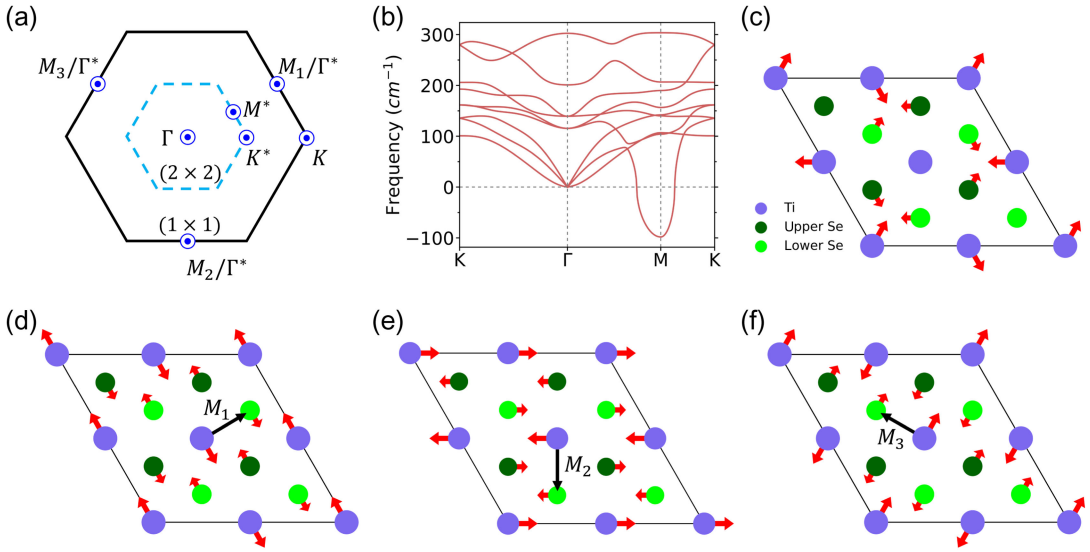

FIG. 1. (a) First Brillouin zones of 1 × 1 (black line) and 2 × 2 (cyan line) $TiSe_2$ monolayer with corresponding high-symmetry points. (b) Phonon dispersion of the unit cell of monolayer $TiSe_2$. (c)–(f) Visualization of the soft phonon mode at (d) M_1, (e) M_2, (f) M_3 point, and (c) their superposition. Purple and green balls represent Ti and Se atoms, respectively. Corresponding atomic displacements and the CDW transition vectors are denoted by the red and black arrows.

The triple-q and single-q modes.—1*T*-$TiSe_2$ exhibits a layered structure with space group $P3\bar{m}1$, where adjacent layers are held together by Van der Waals forces. The first Brillouin zone (BZ) of a single layer $TiSe_2$ is two-dimensional, shown in Fig. 1(a), with three high-symmetry points, Γ, M, and K. There, the three M points M_1, M_2, and M_3 are equivalent due to the in-plane threefold rotational symmetry. Figure 1(b) shows the calculated phonon dispersion of a monolayer $TiSe_2$ unit cell. There is a soft phonon mode emerging at M, indicating a charge ordering in a 2 × 2 supercell with coupled period lattice distortion. As a result, the BZ is reduced [cyan line In Fig. 1(a)] and the normal mode originally at M_i is folded to Γ^* with triple degeneracy. Corresponding eigenmodes are depicted in Figs. 1(d)–1(f), where atomic displacements are transversal to their propagation wave vectors at the three M_i ($i = 1, 2, 3$), constrained by the L_2 irreducible representation [27]. Since the distortion pattern is solely dominated by one M point in BZ, it is called the single-q mode [28]. Further, a superposition of all these three single modes with equal weights leads to a more stable energy profile (by ∼2 meV/f.u.) than the corresponding metastable single-q mode. Therefore, the CDW distortions observed in experiments are likely the high-symmetry phase, or the so called triple-q state [27,28].

Photoinduced chiral CDW phases.—Although the single-q modes have not been detected in experiments, they do provide a unique opportunity to study chirality. Here, we propose to use laser excitation to manipulate transitions among these three metastable CDW states. Specifically, a laser pulse that is polarized along the M_1 plane [red arrows in Fig. 2(a)], can trigger transient nonequilibrium charge distribution and result in further breaking of the intrinsic rotational symmetry in monolayer $TiSe_2$.

In an effort to quantitatively investigate the transient charge order, we simulate the ultrafast response of $TiSe_2$ upon photoexcitation [for details see Supplemental Material (SM), Sec. S1 [29]]. We first observe a charge-density redistribution, as shown in the inset in Fig. 2(b). The differential charge density is defined as $\rho_{\mathrm{tot}}(\boldsymbol{r}, t) = \rho_{\mathrm{chg}}(\boldsymbol{r}, t) - \rho_{\mathrm{atom}}(\boldsymbol{r}, t)$, where $\rho_{\mathrm{chg}}(\boldsymbol{r}, t)$ is the charge density and $\rho_{\mathrm{atom}}(\boldsymbol{r}, t)$ is the superposition of the atomic charge densities. The contour plot of the absolute value $\rho_{\mathrm{tot}}(\boldsymbol{r}, t)$ thus features the distribution of the bonding densities and specifically represents the bonding strength. To track the time evolution of such nonequilibrium charge distribution, we characterize the decomposed bonding strength by partitioning ρ_{tot} into B_{M_1}, B_{M_2}, and B_{M_3} according to the translational symmetry along their corresponding directions (for details see SM, Sec. S2 [29]). As illustrated in Fig. 2(b), upon photoexcitation the bonding charge distributes in an anisotropic way, in which B_{M_2} and B_{M_3} are reduced by about 9% while B_{M_1} is reduced by only 4%. As a result, the threefold rotational symmetry is broken and the structure resides in a single-q dominated bonding pattern. We further calculate the momentum-resolved population of photoexcited charge carriers by projecting the time-dependent Kohn-Sham wave functions ($|\psi_{n,\boldsymbol{k}}(t)\rangle$) onto the basis of the ground-state wave functions ($|\psi_{n',\boldsymbol{k}}(0)\rangle$),

$$\eta_{\boldsymbol{k}}(t) = \sum_{n} \sum_{n'}^{\mathrm{CB}} |\langle \psi_{n',\boldsymbol{k}}(0) | \psi_{n,\boldsymbol{k}}(t) \rangle|^2, \tag{1}$$

where n sums over the band indices and n' runs over all conduction bands. We see from Fig. 2(c) that there are more electrons excited along $\Gamma - M_2$ and $\Gamma - M_3$directions after

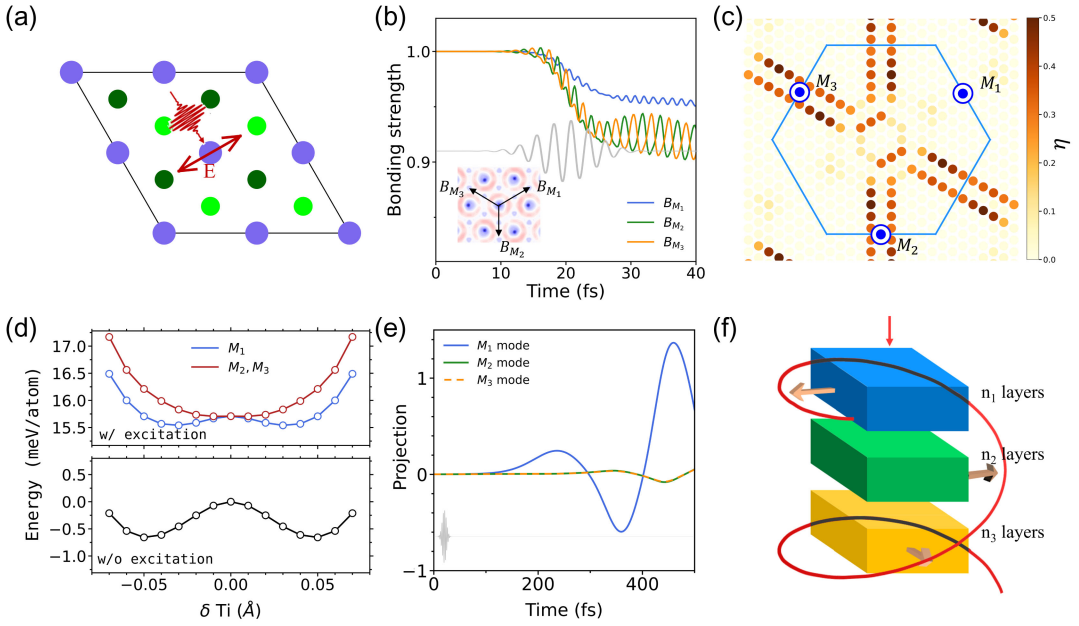

FIG. 2. (a) Schematics of the optical control of phase transition in monolayer $TiSe_2$ *via* a laser pulse [profile shown as the gray line in (b)] linearly polarized along the M_1 direction (red arrow). (b) Time evolution of the bonding strength calculated in a 2×2 $TiSe_2$ supercell. Differential charge density after illumination is shown in the inset. (c) False color representation of the momentum space distribution of the excited electrons after the laser pulse, showing the light selectivity of the three otherwise equivalent directions. (d) The potential energy surface (PES) along the three vibrational modes at M. The upper (lower) panel represents with (without) laser excitations, in which black and colored lines correspondingly denote the ground state PES and nonequilibrium PES. (e) Projected vibrational amplitude of M_1, M_2, and M_3 phonon modes driven by the ultrafast laser pulse (gray line) with a fluence of 0.7 mJ/cm^2. (f) Schematic illustration of the CP-laser-driven chirality. The blue, green, and orange blocks represent three successive slices, which consist of n_1, n_2, and n_3 multilayers of $TiSe_2$, respectively. When a CP light is propagating along the out-of-plane direction of the material, different slices undergo electric fields with varying directions due to the phase shift of the laser between layers.

laser excitation, whereas electronic wave functions along $\Gamma - M_1$ are hardly excited. These results indicate that linearly polarized light leads to promoted carriers along its transverse directions in the momentum space.

Anisotropic charge order would further induce the renormalization of potential energy surface (PES), which we show in Fig. 2(d) along the three single-q phonon modes. The PES exhibits a triply degenerate double-well shape when laser excitation is absent (black line in lower panel) while such degeneracy is lifted upon photoexcitation (colored lines in upper panel). This again shows a rotational symmetry breaking in the ground state, in line with the previous dynamic simulation with a linearly polarized laser pulse. Interestingly, we observe that the PES along M_1 (blue line) maintains a double-well shape, whereas that along M_2 and M_3 (red lines) reshape to a single well. This means the system prefers to be driven into the energy-minimum configuration of the M_1 mode while hardly distorted along M_2 and M_3 directions, thus evidencing coupling between the nonequilibrium electronic system to the lattice degree of freedom.

Now we turn to the excited-state nonequilibrium structural dynamics, where the response of PES would modulate atomic configurations to a transient phase at an ultrafast timescale. The extracted amplitudes of photo-induced single-q modes upon excitation are shown in Fig. 2(e) (for a complete representation of all phonon modes see SM, Sec. S3 [29]). Interestingly, only the M_1 mode is fully excited and coherently vibrates, while M_2 and M_3 modes show negligible amplitude in 500 fs. This is consistent with the static energy profiles calculation in Fig. 2(d), in which the collective mode only oscillates in two wells on the PES along M_1. The combination of the static PES calculation and the time evolution of the atomic motion demonstrates that linearly polarized light can access the interaction-dominated phase space and modulate phase transitions between metastable single-q states.

Taking this idea one step further, we expect that circularly polarized (CP) light to be an efficient means to generate chirality via phase transitions. As schematically shown in Fig. 2(f), supposing a left-handed laser pulse propagating along the z direction of the material can dramatically drive the system far from its static state instantaneously, there may be discrete slices experiencing an effective electric field polarized along different directions. That is to say, the blue slice with n_1 multilayer should experience an electric field pointing at M_3, while the green (yellow) slice with n_2 (n_3) multilayer experiences a field oriented at M_1 (M_2), thus naturally leading to a phase shift between adjacent slices. Since thermal effect would weaken interlayer

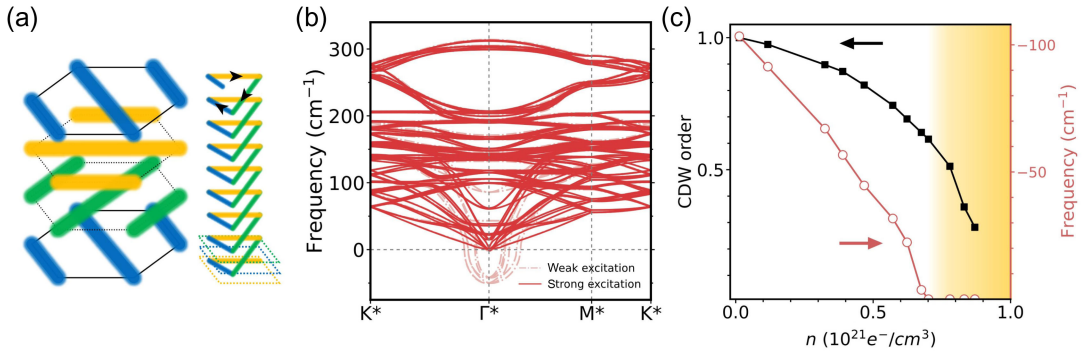

FIG. 3. (a) Schematic representation of the three-layer model (left panel). The yellow, green, and blue planes correspond to single-q patterns along the lowest energy phonon modes at M_1, M_2, and M_3 points, respectively. Charge density distributes in a corkscrew pattern (right panel). (b) Phonon spectrum of the three-layer model at a weak excitation intensity (0.47×10^{21} e$^-$/cm^3, pink) and a strong excitation intensity (0.73×10^{21} e$^-$/cm^3, red). (c) Evolution of the lowest phonon mode frequency at Γ^* and CDW order as a function of excitation intensity n. The strong dependence of both curves signals a chiral CDW transition at a critical point where atomic configuration is fully stabilized in a helical arrangement (shaded area).

couplings [44,45], each slice is likely to respond to the light-imposing external fields independently. As a result, the rotation of electric fields between layers gives a chiral bonding order, and finally results in a chiral coupled electron-lattice system. This proposal, if it works, demonstrates a scenario of chirality transfer from light to the electron subsystem, and then to the lattice degree of freedom.

A three-dimensional chiral CDW phase.—To explore the feasibility of such laser modulation, we build a model system whose "unit cell" consists of three $TiSe_2$ layers to mimic the successive slices shown in Fig. 2(f). As visualized in Fig. 3(a), each layer exhibits a single-q pattern, and by launching a chiral structure with either an $M_1 - M_2 - M_3$ or an $M_1 - M_3 - M_2$ sequence, the model can in principle capture distinctive features in comparison to the achiral CDW phase.

To evaluate the stability of the composed model, we carry out phonon dispersion calculations employing a variety of electronic smearing parameters σ, which characterizes the electron temperature and can practically represent the excitation intensity n in the context of excited states (for details see SM, Sec. S4 [29]), since the laser excited hot carriers can thermalize to a quasi Fermi-Dirac distribution at a timescale much shorter than the relaxation of other degrees of freedom. As depicted in Fig. 3(b), the imaginary phonon modes at M points are now folded to the zone center in the 2×2 supercell, and show up as the lowest modes at Γ^*. Upon varying σ, we can qualitatively monitor the frequency change of these unstable phonon modes and thus the structural stability with respect to excitation intensity. At a lower excitation intensity of $n = 0.47 \times 10^{21}$ e$^-$/cm^3 (pink curve), it is obvious that the system is dynamically unstable with large imaginary frequencies. With higher excitation intensity of $n = 0.73 \times 10^{21}$ e$^-$/cm^3 (red curve), the imaginary phonon frequencies are eliminated, indicating that the three-layer model can be stabilized with intense excitation.

To reveal the correlation between the excitation intensity and the structural instability, we obtain both the phonon frequencies (red curve) and CDW order parameters δ_{Ti} (black curve) under various n, the latter defined as the titanium atomic displacements normalized by that at 0 K (δ_0). As shown in Fig. 3(c), the CDW is highly ordered with a corkscrew pattern at lower n, while the corresponding imaginary phonon frequency is too large ($\sim$100 cm^{-1}) for a structure to be dynamically stable. It further shows the concordance of the structural stability (red curve) and CDW order (black curve) with respect to the excitation intensity. Increasing the laser intensity weakens the lattice distortion and hardens the lowest phonon modes in the mean time. Importantly, the imaginary phonon frequency decays at a faster rate than the order parameter. At the threshold of $n = 0.7 \times 10^{21}$ e$^-$/cm^3, the model is still trapped in a helical structure with a finite single-q distortion ($\approx 0.6\delta_0$) of each constituent layer, while the phonon modes become fully stabilized by coupling with the hot electrons. Moreover, such a chiral state can be maintained even up to a higher n of 0.9×10^{21} e$^-$/cm^3, shown by the shaded region. We thus propose that such a chiral CDW structure can be practically driven and stabilized by a circularly polarized laser with a certain excitation intensity.

Discussion.—Finally, we characterize possible signatures of our model to verify its chirality. One is the circular photogalvanic effect [20,46,47], which drives current along opposite directions for light with different chirality. In our simulations, a circularly polarized laser is incident along the out-of-plane direction of the chiral $TiSe_2$, inducing a photocurrent illustrated by the orange arrow in Fig. 4(a). The light-induced photocurrent can be obtained by

$$J(t) = \frac{1}{2i}\int_{\Omega} d\boldsymbol{r} \sum_i \{\psi_i^*(\boldsymbol{r},t)\nabla\psi_i(\boldsymbol{r},t) - \psi_i(\boldsymbol{r},t)\nabla\psi_i^*(\boldsymbol{r},t)\}, \tag{2}$$

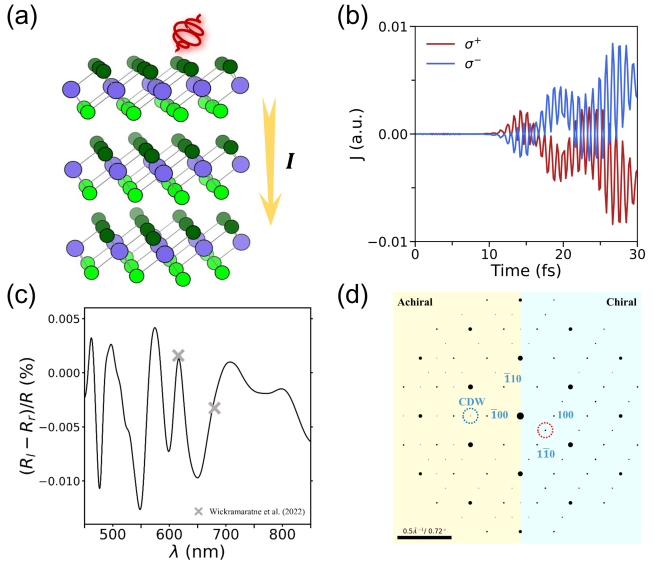

FIG. 4. (a) Schematic illustration of the circular photogalvanic effect. A photocurrent I along the z direction is induced by a circularly polarized light. (b) Transient circular photogalvanic current as a function of time for an 800 nm pump. (c) Degree of chirality $(R_r - R_l)/R$ as a function of photon wavelength calculated for the three-layer model. The two gray markers denote experimental observations from Ref. [19]. (d) Simulated electron diffraction patterns for the achiral and chiral CDW phases.

where ψ_i is real-time wave function of the ith occupied eigenstate. Photocurrent along z direction is displayed in Fig. 4(b) for both σ_+ and σ_- lasers with a wavelength of 800 nm. The circular dichroism effect can be clearly seen by the two signals with the same magnitude but opposite signs. Further, the degree of chirality can be calculated as $(R_r - R_l)/R$, where R_r (R_l) and R correspond to right (left) circular polarized reflectivity and their averaged value, at a wide range of wavelengths (for details see SM, Sec. S5 [29]). As shown in Fig. 4(c), the degree of chirality is predicted to be positive between 570 and 640 nm, and negative between 520 and 570 nm and between 640 and 690 nm. We find that the signs of the spectrum at 620 and 680 nm coincide with previous work [19] (gray symbols), though it does not show a full agreement quantitatively. Finally, the new emerging gyrotropic state may be macroscopically verified by electron diffraction. We simulate the diffraction patterns for both achiral [19] and chiral phases. For the latter we use a single-q mode monolayer to enhance the surface effect. In Fig. 4(d), the left panel shows the pattern of the achiral phase, where a diffraction peak between $[\bar{1}00]$ and $[\bar{2}00]$ emerges (blue circle), indicating a typical CDW phase wave vector at M. However, in the right panel, the CDW peak disappears while an emergent $[1\frac{\bar{1}}{2}0]$ spot with nematic arrangement can be clearly seen and attributed to the signature of chiral CDW phases.

Conclusions.—We provide a theoretical investigation of the photoinduced symmetry breaking and chiral CDW phase in $TiSe_2$ using rt-TDDFT and Ehrenfest molecular dynamics simulations. In the monolayer limit, we find the CDW phase corresponds to a 2×2 supercell, and arises from the superposition of triply degenerate soft modes at the M point. Upon laser excitation, the charge redistributes anisotropically and thus eliminates the threefold rotational symmetry. In accompany, the potential energy surface evolves to a single-well shape along the two transverse directions with respect to the light polarization, while keeping a double-well shape along the selected direction and thus leading to a single-q dominated lattice distortion. We then construct a model structure with three successive single-q patterned $TiSe_2$ layers and thus forming a chiral lattice. By simulating its phonon dispersion with varying excitation intensities, we show that it can be stabilized with a moderate CDW order due to the coupled chiral electron-lattice system. We further propose circularly polarized light as an effective method to induce and manipulate chirality in $TiSe_2$. Together these findings serve as a theoretical ground for understanding, realizing, and manipulating chirality and its coupling to the electron and lattice subsystems, which we hope will inspire future experimental explorations of optical control of chirality in quantum materials.

The authors thank the Ministry of Science and Technology (No. 2021YFA1400201), National Natural Science Foundation of China (No. 12025407, No. 11934004, and No. 92250303), and Chinese Academy of Sciences (No. YSBR-047 and No. XDB33030100) for financial support.

*Corresponding author: yaxianw@iphy.ac.cn
†Corresponding author: smeng@iphy.ac.cn

[1] R. E. Peierls, *Quantum Theory of Solids* (Oxford University Press, New York, 1955).
[2] J. Friedel, in *Electron-Phonon Interactions and Phase Transitions* (Springer US, New York, 1977), pp. 1–49.
[3] X. Teng, J. S. Oh, H. Tan, L. Chen, J. Huang, B. Gao, J.-X. Yin, J.-H. Chu, M. Hashimoto, D. Lu, C. Jozwiak, A. Bostwick, E. Rotenberg, G. E. Granroth, B. Yan, R. J. Birgeneau, P. Dai, and M. Yi, Nat. Phys. **19**, 814 (2023).
[4] S. Ramakrishnan, A. Schönleber, T. Rekis, N. van Well, L. Noohinejad, S. van Smaalen, M. Tolkiehn, C. Paulmann, B. Bag, A. Thamizhavel, D. Pal, and S. Ramakrishnan, Phys. Rev. B **101**, 060101 (2020).
[5] F. Qin, S. Li, Z. Z. Du, C. M. Wang, W. Zhang, D. Yu, H.-Z. Lu, and X. C. Xie, Phys. Rev. Lett. **125**, 206601 (2020).
[6] Y. Zhong, J. Liu, X. Wu, Z. Guguchia, J.-X. Yin, A. Mine, Y. Li, S. Najafzadeh, D. Das, C. Mielke, R. Khasanov, H. Luetkens, T. Suzuki, K. Liu, X. Han, T. Kondo, J. Hu, S. Shin, Z. Wang, X. Shi, Y. Yao, and K. Okazaki, Nature (London) **617**, 488 (2023).

[7] Y. Song, T. Ying, X. Chen, X. Han, X. Wu, A. P. Schnyder, Y. Huang, J.-g. Guo, and X. Chen, Phys. Rev. Lett. **127**, 237001 (2021).

[8] E. Morosan, H. W. Zandbergen, B. S. Dennis, J. W. G. Bos, Y. Onose, T. Klimczuk, A. P. Ramirez, N. P. Ong, and R. J. Cava, Nat. Phys. **2**, 544 (2006).

[9] H. D. Flack, Helv. Chim. Acta **86**, 905 (2003).

[10] G. H. Wagnière, *On Chirality and the Universal Asymmetry: Reflections on Image and Mirror Image* (John Wiley & Sons, New York, 2007).

[11] L. Fu, Phys. Rev. Lett. **115**, 026401 (2015).

[12] P. Hosur, A. Kapitulnik, S. A. Kivelson, J. Orenstein, and S. Raghu, Phys. Rev. B **87**, 115116 (2013).

[13] J. Orenstein and J. E. Moore, Phys. Rev. B **87**, 165110 (2013).

[14] J. van Wezel, Europhys. Lett. **96**, 67011 (2011).

[15] J.-P. Castellan, S. Rosenkranz, R. Osborn, Q. Li, K. E. Gray, X. Luo, U. Welp, G. Karapetrov, J. P. C. Ruff, and J. van Wezel, Phys. Rev. Lett. **110**, 196404 (2013).

[16] M. Iavarone, R. Di Capua, X. Zhang, M. Golalikhani, S. A. Moore, and G. Karapetrov, Phys. Rev. B **85**, 155103 (2012).

[17] J. Ishioka, T. Fujii, K. Katono, K. Ichimura, T. Kurosawa, M. Oda, and S. Tanda, Phys. Rev. B **84**, 245125 (2011).

[18] J. Ishioka, Y. H. Liu, K. Shimatake, T. Kurosawa, K. Ichimura, Y. Toda, M. Oda, and S. Tanda, Phys. Rev. Lett. **105**, 176401 (2010).

[19] D. Wickramaratne, S. Subedi, D. H. Torchinsky, G. Karapetrov, and I. I. Mazin, Phys. Rev. B **105**, 054102 (2022).

[20] S.-Y. Xu, Q. Ma, Y. Gao, A. Kogar, A. Zong, A. M. M. Valdivia, T. H. Dinh, S.-M. Huang, B. Singh, C.-H. Hsu, T.-R. Chang, J. P. C. Ruff, K. Watanabe, T. Taniguchi, H. Lin, G. Karapetrov, D. Xiao, P. Jarillo-Herrero, and N. Gedik, Nature (London) **578**, 545 (2020).

[21] J. J. Gao, W. H. Zhang, J. G. Si, X. Luo, J. Yan, Z. Z. Jiang, W. Wang, H. Y. Lv, P. Tong, W. H. Song, X. B. Zhu, W. J. Lu, Y. Yin, and Y. P. Sun, Appl. Phys. Lett. **118**, 213105 (2021).

[22] I. Guillamón, H. Suderow, J. G. Rodrigo, S. Vieira, P. Rodière, L. Cario, E. Navarro-Moratalla, C. Martí-Gastaldo, and E. Coronado, New J. Phys. **13**, 103020 (2011).

[23] A. Zong, X. Shen, A. Kogar, L. Ye, C. Marks, D. Chowdhury, T. Rohwer, B. Freelon, S. Weathersby, R. Li, J. Yang, J. Checkelsky, X. Wang, and N. Gedik, Sci. Adv. **4**, eaau5501 (2018).

[24] X. Song, L. Liu, Y. Chen, H. Yang, Z. Huang, B. Hou, Y. Hou, X. Han, H. Yang, Q. Zhang, T. Zhang, J. Zhou, Y. Huang, Y. Zhang, H.-J. Gao, and Y. Wang, Nat. Commun. **13**, 1843 (2022).

[25] Y.-X. Jiang *et al.*, Nat. Mater. **20**, 1353 (2021).

[26] J. van Wezel and P. Littlewood, Physics **3**, 87 (2010).

[27] F. J. Di Salvo, D. E. Moncton, and J. V. Waszczak, Phys. Rev. B **14**, 4321 (1976).

[28] R. Bianco, M. Calandra, and F. Mauri, Phys. Rev. B **92**, 094107 (2015).

[29] See Supplemental Material at http://link.aps.org/supplemental/10.1103/PhysRevLett.131.196401 for detailed discussions on the bonding strength, the projection of all phonon modes, the excitation density, the optical chirality, and computational details, etc., which includes Refs. [14,19,30–43].

[30] G. Kresse and J. Hafner, Phys. Rev. B **47**, 558 (1993).

[31] G. Kresse and J. Furthmüller, Phys. Rev. B **54**, 11169 (1996).

[32] L. Chaput, A. Togo, I. Tanaka, and G. Hug, Phys. Rev. B **84**, 094302 (2011).

[33] A. Togo and I. Tanaka, Scr. Mater. **108**, 1 (2015).

[34] H. J. Monkhorst and J. D. Pack, Phys. Rev. B **13**, 5188 (1976).

[35] C. Lian, M. Guan, S. Hu, J. Zhang, and S. Meng, Adv. Theory Simul. **1**, 1800055 (2018).

[36] W. Ma, J. Zhang, L. Yan, Y. Jiao, Y. Gao, and S. Meng, Comput. Mater. Sci. **112**, 478 (2016).

[37] S. Meng and E. Kaxiras, J. Chem. Phys. **129**, 054110 (2008).

[38] M. Noda, S. A. Sato, Y. Hirokawa, M. Uemoto, T. Takeuchi, S. Yamada, A. Yamada, Y. Shinohara, M. Yamaguchi, K. Iida, I. Floss, T. Otobe, K.-M. Lee, K. Ishimura, T. Boku, G. F. Bertsch, K. Nobusada, and K. Yabana, Comput. Phys. Commun. **235**, 356 (2019).

[39] C. Pemmaraju, F. Vila, J. Kas, S. Sato, J. Rehr, K. Yabana, and D. Prendergast, Comput. Phys. Commun. **226**, 30 (2018).

[40] G. Kresse and D. Joubert, Phys. Rev. B **59**, 1758 (1999).

[41] J. P. Perdew, K. Burke, and M. Ernzerhof, Phys. Rev. Lett. **77**, 3865 (1996).

[42] C. Riekel, J. Solid State Chem. **17**, 389 (1976).

[43] J. van Wezel, J. Phys. Conf. Ser. **391**, 012167 (2012).

[44] S. Huang, F. Wang, G. Zhang, C. Song, Y. Lei, Q. Xing, C. Wang, Y. Zhang, J. Zhang, Y. Xie, L. Mu, C. Cong, M. Huang, and H. Yan, Phys. Rev. Lett. **125**, 156802 (2020).

[45] S. Tongay, J. Zhou, C. Ataca, K. Lo, T. S. Matthews, J. Li, J. C. Grossman, and J. Wu, Nano Lett. **12**, 5576 (2012).

[46] V. M. Asnin, A. A. Bakun, A. M. Danishevskii, E. L. Ivchenko, G. E. Pikus, and A. A. Rogachev, JETP Lett. **28**, 74 (1978), http://jetpletters.ru/ps/1557/article_23830.pdf.

[47] V. Asnin, A. Bakun, A. Danishevskii, E. Ivchenko, G. Pikus, and A. Rogachev, Solid State Commun. **30**, 565 (1979).